

Article

Compression of the Synchrotron Mössbauer X-ray Photon Waveform in an Oscillating Resonant Absorber

Ilias R. Khairulin ^{1,*}, Yevgeny V. Radeonychev ¹ and Olga Kocharovskaya ²¹ Institute of Applied Physics of the Russian Academy of Sciences, 46 Ulyanov Street, 603950 Nizhny Novgorod, Russia² Department of Physics and Astronomy, Texas A&M University, 578 University Drive, College Station, TX 77843-4242, USA

* Correspondence: khairulinir@ipfran.ru

Abstract: A technique to transform the waveform of a 14.4 keV photon (time dependence of the photon detection probability or, equivalently, the intensity of the single-photon wave packet) into a regular sequence of short, nearly bandwidth-limited pulses with a controlled number of pulses is proposed. It is based on coherent forward scattering of single X-ray photons from a synchrotron Mössbauer source (SMS) in an optically thick, vibrating, recoilless ^{57}Fe resonant absorber. The possibility of compressing the waveform of an SMS photon into a single short bell-shaped pulse is predicted. The experiment is proposed for compressing a 100 ns duration 14.4 keV single-photon wave packet produced by SMS at the European Synchrotron Radiation Facility (ESRF) into a single bell-shaped pulse of less than 20 ns duration and more than twice the peak intensity. Such single-photon coherent pulses are promising for applications in the fast-developing field of X-ray quantum optics, including possible implementation of quantum memory.

Keywords: X-ray photons; synchrotron Mössbauer source; pulse compression

Citation: Khairulin, I.R.; Radeonychev, Y.V.; Kocharovskaya, O. Compression of the Synchrotron Mössbauer X-ray Photon Waveform in an Oscillating Resonant Absorber. *Photonics* **2022**, *9*, 829. <https://doi.org/10.3390/photonics9110829>

Received: 14 September 2022

Accepted: 31 October 2022

Published: 4 November 2022

Publisher's Note: MDPI stays neutral with regard to jurisdictional claims in published maps and institutional affiliations.



Copyright: © 2022 by the authors. Licensee MDPI, Basel, Switzerland. This article is an open access article distributed under the terms and conditions of the Creative Commons Attribution (CC BY) license (<https://creativecommons.org/licenses/by/4.0/>).

1. Introduction

The methods of generation of coherent electromagnetic radiation in the form of a single short pulse or a given number of pulses in various spectral ranges from terahertz up to X-rays have been intensively developed during the last decades. In the X-ray range, radiation pulses with the photon energy of 14.4 keV find numerous applications owing to the availability of sources of such radiation and the variety of media in which ^{57}Fe nuclei resonant to 14.4 keV photons can be imbedded [1–4]. The 14.4 keV pulses are typically generated by the radioactive ^{57}Co nuclide and synchrotrons after proper narrowing of extremely broadband X-ray bursts emitted from the synchrotron storage ring [3,4]. The main feature of both types of sources is normally the emission, on average, of less than one photon per pulse duration. In other words, such pulses are single-photon pulses. Their spectral and temporal characteristics are obtained as a result of multiply repeated detection of single photons.

In the case of a ^{57}Co radioactive source, the stochastic emission of a 122 keV photon precedes an emission of a 14.4 keV photon [4]. Therefore, the measurement of the temporal characteristics of the 14.4 keV single-photon pulse begins from the moment of detection of a 122 keV photon (which can be assumed as $t = 0$). This detection event indicates that some ^{57}Co nucleus of the source has radioactively decayed and converted into a ^{57}Fe nucleus in the excited energy state of the 14.4 keV quantum transition, making possible the emission of the 14.4 keV photon. Then, the time interval that has elapsed from the moment when the emission of the 14.4 keV photon became possible ($t = 0$) to the moment of its detection is measured. This procedure is repeated many times. As a result, the dependence of the number of detected 14.4 keV photons on the time elapsed since $t = 0$ (or the time dependence of the 14.4 keV photon detection probability) is measured. The whole set of the

14.4 keV photon detection moments forms a single-photon wave packet or a single-photon pulse. The measured time dependence of the 14.4 keV photon detection probability is the photon waveform that is proportional to the intensity of the single-photon wave packet (single-photon pulse).

In the case of a synchrotron-based source of the 14.4 keV photons, the emission of the 14.4 keV photon becomes possible starting from the moment of emission of an X-ray pulse from the synchrotron storage ring, which defines $t = 0$ [3]. Otherwise, the waveform of the photon is measured in the same manner as in the case of the radioactive source.

The measurement of the spectral characteristics of the 14.4 keV single-photon pulse from both types of sources is similar to that discussed above and is based on the multiply recorded carrier frequency of the detected photons. The result is the dependence of the number of detected photons in a given frequency bin on the bin frequency or, equivalently, the frequency dependence of the photon detection probability, or the squared spectral amplitude of the single-photon pulse.

The ^{57}Co source during recoilless (Mössbauer) emission produces the 14.4 keV coherent bandwidth-limited single-photon exponential pulse. Its full duration at half maximum (FDHM) is about 98 ns. The main feature of this pulse is the stepwise front edge corresponding to the Lorentzian spectral contour. When such a pulse propagates through the resonant recoilless (Mössbauer) medium, its front edge does not change. Such a front edge can be neither stored in the nuclear coherence nor reshaped by the medium. This restricts applications of the Lorentzian single-photon pulses. A gradual increase in the nuclear response due to the field following the stepwise front edge of the Lorentzian pulse causes a specific alteration of its initial part, called the Sommerfeld–Brillouin precursor. Due to the Sommerfeld–Brillouin precursor, the Lorentzian single-photon pulse cannot be compressed into a short single pulse with a smooth envelope. The shortening of the Sommerfeld–Brillouin precursor is possible via transmission of a 14.4 keV Lorentzian single-photon pulse through a resonant, optically deep medium of ^{57}Fe recoilless nuclei [5]. In this case, a short Sommerfeld–Brillouin precursor of the transmitted photon waveform, known as the speed-up effect, has the stepwise front edge and is followed by a long and weak tail of oscillating intensity, called the dynamical beats [6].

Another method for obtaining a short burst within the 14.4 keV Lorentzian single-photon pulse is based on the rapid reversal of the nuclear response phase with respect to the phase of the incident field via fast displacement of the absorber relative to the source by a half wavelength of the photon [7,8]. This changes the destructive interference between the nuclear response and the incident field (causing the absorption of pulse) to the constructive interference, leading to a burst of intensity in the transmitted photon waveform. The appearance moment of the burst is determined by the moment of the absorber displacement. The burst duration is limited by the duration of the absorber displacement, the decay rate of the nuclear coherence, and the absorber Mössbauer thickness (optical depth of recoilless absorption). In this case, the burst of intensity always follows the Sommerfeld–Brillouin precursor. In other words, the minimum number of pulses into which the exponential waveform of the incident photon can be transformed by this method is two.

The 14.4 keV Lorentzian single-photon pulses from a ^{57}Co source can be transformed into a regular sequence of short pulses via transmission of the photons through the properly vibrated recoilless ^{57}Fe resonant nuclear absorber implemented in [9,10]. However, the stochastic emission of the photons does not allow to lock the time moment $t = 0$ to some phase of the absorber vibration. As a result, the whole ensemble of photons at the exit from the vibrated absorber constitutes an infinite number of different single-photon short-pulse sequences produced at different absorber vibration phases. The observation of a selected short-pulse sequence was implemented in [9,10] via a stroboscopic-like technique when only 14.4 keV photons corresponding to a certain phase of the absorber vibration were counted. Hence, the selected 14.4 keV single-photon wave packet was not actually produced at the exit from the absorber and, therefore, has limited applications.

The 14.4 keV single-photon pulses produced by the synchrotron-based sources are not bandwidth-limited. They normally have on the order of tens of picoseconds duration, corresponding to a Fourier transform-limited spectral width on the order of tens of gigahertz. At the same time, the measured spectral width of these pulses is several terahertz since the energy of photons fluctuates around 14.4 keV [1–3]. However, each separate photon interacts with the nuclei as a coherent bandwidth-limited pulse of the electromagnetic field. The linewidth of the recoilless resonant 14.4 keV transition of ^{57}Fe normally ranges from 1.13 to several MHz. Therefore, 14.4 keV synchrotron photons interact with ^{57}Fe nuclei as a delta-like pulse. This is the basis for the widely used time domain Mössbauer spectroscopy with synchrotron radiation (SR). A number of experiments in the field of quantum optics with SR photons should be noted, namely, storage of nuclear excitation energy [11], observation of superradiance collective lamb shift [12], electromagnetically induced transparency of 14.4 keV photons in a nano-scale cavity with embedded ^{57}Fe nuclei [13], Rabi oscillations between two nuclear ensembles [14], and X-ray control of nuclear states [15], etc. However, such an X-ray single-photon pulse is usually too short to be used for quantum information processing, for example, to store it in the medium and retrieve on demand.

One more source of 14.4 keV single photons should be pointed out, namely, the synchrotron Mössbauer source (SMS). Currently, there are two SMSs, located at the European Synchrotron Radiation Facility (ESRF) [16] and the Spring-8 facility [17]. The SMS is especially well-suited for studies of small (micron size) samples that are difficult or impossible to perform with a conventional radioactive source, for example, studies of various minerals under very high-pressure conditions in the Earth's lower mantle [18–20]. The SMS constitutes a near-perfect $^{57}\text{FeBO}_3$ (iron borate) single crystal. Due to the pure nuclear reflection near the Bragg angle, iron borate can transform the X-ray bursts from the synchrotron storage ring into single 14.4 keV photons, similar to photons from the ^{57}Co source [16,17,21–24]. The typical duration and spectral width of the SMS nearly bandwidth-limited single-photon pulse are about 100 ns and 3 MHz, respectively. The spectral and temporal characteristics of the SMS 14.4 keV photons can be varied depending on the temperature of the $^{57}\text{FeBO}_3$ crystal, its angular position relative to the incident SR beam, as well as on the applied external constant and radiofrequency magnetic fields [16,17,21–24].

One of the main advantages of the SMS over the ^{57}Co Mössbauer source is the ability to produce a single-photon pulse with a smooth front edge. As a result, the waveform of such SMS photon transmitted through a resonant medium does not contain the Sommerfeld–Brillouin precursor. This opens the possibility of compressing the SMS photon waveform into a single short pulse with a smooth bell-shaped envelope and a duration suitable for quantum optics applications.

Another important advantage of the SMS compared to the radioactive source is the possibility to synchronize the emission of 14.4 keV photons from the synchrotron storage ring with a certain phase of the absorber vibration. This makes it possible to use the entire photon flux to generate one specific single-photon wave packet in the form of a short-pulse sequence.

As we show in this paper, transmission of the SMS photons through the vibrating resonant absorber allows for producing a single-photon wave packet in the form of a short-pulse sequence with an arbitrary number of nearly bandwidth-limited short pulses. We also propose an experiment to compress a 100 ns-length 14.4 keV single-photon pulse from SMS into a bell-shaped nearly bandwidth-limited single pulse of less than 20 ns in duration. Contrary to short pulses normally produced by synchrotrons (on the order of picoseconds) and to long pulses (on the order of 100 ns) produced by the radioactive or synchrotron Mössbauer sources, the bell-shaped pulse of such an intermediate duration can be stored in the nuclear coherence of an ensemble of the nuclei and subsequently retrieved on demand, as proposed in [25], i.e., used for implementation of a quantum nuclear memory.

The paper is organized as follows. Section 2 describes the theoretical model. In Section 3, we develop an analytical model in the case of a high frequency of the absorber

vibration and discuss the basic mechanism for the short-pulse formation. In Section 4, we find numerically experimental conditions for compressing the Lorentz-squared single-photon wave packet emitted by ESRF SMS into a single short, nearly bandwidth-limited pulse with increased peak intensity or, on demand, into two or three pulses with controlled relative peak intensities. In Section 5, we summarize the results.

2. Theoretical Model

Let us consider the electromagnetic field of a 14.4 keV single-photon pulse emitted by SMS available at ESRF [16,21–23]. If the $^{57}\text{FeBO}_3$ crystal is heated in an external magnetic field to the Néel temperature, the multilane Mössbauer radiation produced via scattering of the SR pulse by the ^{57}Fe nuclei can collapse into a single spectral line, similar to the spectral line of 14.4 keV radiation emitted by the ^{57}Co radioactive source [16,17,21–24]. The produced quasi-monochromatic, nearly bandwidth-limited single-photon pulse is the result of several mechanisms of interaction between the SR and a lattice of oriented ^{57}Fe nuclear spins [16,21–23]. It has a non-Lorentzian spectral shape, which is determined by the temperature of the $^{57}\text{FeBO}_3$ crystal, its angular position relative to the incident beam near the Bragg angle, and the applied magnetic fields [16,17,21–24]. Accordingly, the shape and duration of the single-photon waveform can be varied in a controllable manner. In implemented cases, the measured SMS photon waveform has a gradually increased front, while the spectral line is several times wider than the radioactive source line at room temperature. Both features can be favorable for some applications, including quantum information processing.

Let us consider one of the SMS photon waveforms obtained in [16,21–23]. The spectrum of this single-photon pulse can be represented as a doublet line constituting a superposition of two close homogeneously broadened antiphase Lorentzian spectral lines:

$$\tilde{E}_S(\omega) = \frac{E_0 e^{i\varphi}}{2\pi\gamma_S} \left[\frac{1}{1 + i(\omega_{SC} - \Delta/2 - \omega)/\gamma_S} - \frac{1}{1 + i(\omega_{SC} + \Delta/2 - \omega)/\gamma_S} \right], \quad (1)$$

where Δ is the detuning of the Lorentzian contours from the central frequency, ω_{SC} ($\hbar\omega_{SC} = 14.4$ keV), corresponding to the wavelength $\lambda_{SC} = 0.86\text{\AA}$, γ_S is the half-width of each Lorentzian contour, E_0 is the amplitude, and φ is the random initial phase of the field, respectively. If the Lorentzian contours are close to each other, so that $\Delta/\gamma_S \ll 1$, then the resulting spectral line of the SMS is close to a pseudo-single spectral line with the Lorentz-squared shape,

$$\tilde{E}_S(\omega) \stackrel{\Delta \ll \gamma_S}{\approx} \frac{E_0}{2\pi\gamma_S} \frac{\Delta/\gamma_S}{[1 + i(\omega_{SC} - \omega)/\gamma_S]^2}. \quad (2)$$

The parameter values of field (1) were determined in [21–23]. They are $\gamma_S \simeq 2.35\Gamma_0$ (where $\Gamma_0/(2\pi) = 1.13$ MHz is the natural linewidth of the ^{57}Fe resonant transition) and $\Delta \simeq 0.94\Gamma_0$. In this case, $\Delta/\gamma_S \simeq 0.4$, so that the condition for the Lorentz-squared spectral line is met rather poorly. Nevertheless, the spectral line, $|\tilde{E}_S(\omega)|^2$, of the field (1) looks as like a single contour (Figure 1a). For brevity, we will call this field the Lorentz-squared single-photon pulse. The full-width at half maximum (FWHM) of this SMS Lorentz-squared spectral line is about 3.6 times larger than the FWHM of the Lorentzian spectral line, $|\tilde{E}_{\text{Co}}(\omega)|^2$, emitted by the ^{57}Co source, where

$$\tilde{E}_{\text{Co}}(\omega) = \frac{E_{\text{Co}}}{\pi\Gamma_0} \frac{1}{1 + 2i(\omega_{SC} - \omega)/\Gamma_0}, \quad (3)$$

E_{Co} is the field amplitude of the Lorentzian contour. The Lorentz-squared spectral line has faster decreasing wings.

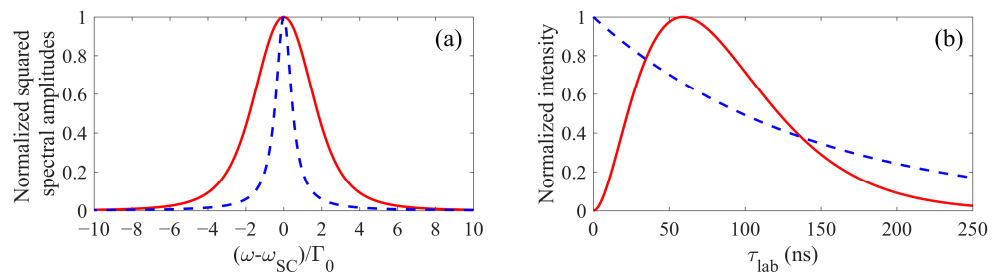


Figure 1. Normalized spectrum (a) and normalized intensity (b) of the ESRF SMS Lorentz-squared single-photon wave packet (the red solid lines) compared to the ^{57}Co Lorentzian single-photon wave packet (the blue dashed lines). In (a), the red solid line, $|\tilde{E}_S(\omega)|^2$, is plotted according to (1), and the blue dashed line, $|\tilde{E}_{\text{Co}}(\omega)|^2$, is plotted according to (3). In (b), the red solid line, $|E_S(\tau_{lab})|^2$, is plotted according to (4), and the blue dashed line, $|E_{\text{Co}}(\tau_{lab})|^2$, is plotted according to (5). For all curves, $\Gamma_0/(2\pi) = 1.13$ MHz, $\gamma_S = 2.35\Gamma_0$, and $\Delta = 0.94\Gamma_0$.

Spectrum (1) corresponds to the following dependence of the electric field on time:

$$\begin{aligned} E_S(\tau_{lab}) &= \int_{-\infty}^{\infty} \tilde{E}_S(\omega) e^{-i\omega\tau_{lab}} d\omega = E_0 e^{i\varphi} \theta(\tau_{lab}) e^{-\gamma_S \tau_{lab}} (e^{-i\omega_1 \tau_{lab}} - e^{-i\omega_2 \tau_{lab}}) \\ &= 2iE_0 e^{i\varphi} \theta(\tau_{lab}) \sin\left(\frac{\Delta}{2} \tau_{lab}\right) e^{-(i\omega_{SC} + \gamma_S) \tau_{lab}}, \end{aligned} \quad (4)$$

where $\tau_{lab} = t - z_{lab}/c$ is the local time in the laboratory reference frame, $\theta(t)$ is the Heaviside step function, $\omega_1 = \omega_{SC} - \Delta/2$, and $\omega_2 = \omega_{SC} + \Delta/2$. It constitutes a quasi-monochromatic wave packet, with the intensity presented in Figure 1b by the red solid curve. The FDHM of the Lorentz-squared single-photon pulse emitted by SMS of ESRF is about 100 ns. This is close to the FDHM of about 98 ns of the exponentially decreasing Lorentzian wave packet,

$$E_{\text{Co}}(\tau_{lab}) = E_{\text{Co}} e^{i\varphi} \theta(\tau_{lab}) e^{-\Gamma_0 \tau_{lab}/2} e^{-i\omega_{SC} \tau_{lab}}, \quad (5)$$

emitted by the ^{57}Co source. At the same time, the stepwise front edge, inherent in the Lorentzian pulse, is absent in the waveform of the Lorentz-squared photon.

Similar to the method proposed in [26,27] and realized in [9,10] for the compression of 14.4 keV Lorentzian photons (the blue dashed lines in Figure 1) emitted by the ^{57}Co source into the pulse sequence, we assume that the 14.4 keV photons from SMS propagate through a recoilless ^{57}Fe resonant absorber oscillating as a whole (piston-like) along the direction of the photon propagation, z_{lab} . In the experiment, the ^{57}Fe absorber is a stainless-steel foil enriched with ^{57}Fe resonant nuclei and fixed on a piezoelectric transducer [9,10,28–33]. The transducer is normally a polyvinylidene fluoride film providing ultrasonic vibration of all ^{57}Fe nuclei with the same amplitude, R , frequency, Ω , and the initial phase, ϑ , within the photon beam [9,10,30,31,33]. Namely, one can write:

$$z_{lab} = z_a + R \sin(\Omega t + \vartheta), \quad (6)$$

where z_a is the coordinate in the vibrating reference frame. In Equation (6), we assume that the thickness of the foil is much smaller than the wavelength of sound in stainless-steel, as well as the absorber's motion is nonrelativistic. Both approximations are satisfied for the absorber considered below (see also [34]). The experimental scheme that we propose is similar to the scheme realized in [9,10].

The initial vibration phase of the absorber, ϑ , should be locked to the front edge of the single-photon wave packet. This makes it possible to modify the nuclear response by the absorber vibration in a coherent manner. In the experiments [9,10] with the ^{57}Co source, the absorber initial vibration phase, ϑ , was locked to the front edge of the single-photon wave packet by means of the selective (stroboscopic-like) detection of stochastically emitted

14.4 keV photons, when only those photons were collected, the possibility of emission of which (determined by the detection of 122 keV photons) appeared at the absorber vibration phase, ϑ . However, the selection of the emitted 14.4 keV photons before the absorber was not performed. As a result, the entire photon stream transmitted through the absorber constituted an infinite set of single-photon wave packets, for each of which the phase ϑ was different and averaged over the set. This technique allows observing the certain waveform of the transmitted photons, but it did not allow to actually produce the photons with the observed waveform.

In the case of SMS, the moments, when the possibility of emission of 14.4 keV photons appears ($t = 0$ corresponding to the beginning of the single-photon wave packet), are the moments of emission of the SR pulse from the synchrotron storage ring. These moments are determined by the revolution frequency of the electronic bunches. Hence, all photons produced by the SMS form the same single-photon wave packet that can be locked to an arbitrary selected value, ϑ , if the absorber vibration frequency is a multiple of the SR pulse repetition rate [31]. This means that the photons with the controllable waveform can actually be produced and can be used for quantum information processing, for example, for realization of a quantum memory by the method proposed in [25].

As shown in [9,33–36], the propagation of a single-photon wave packet through the oscillating resonant recoilless absorber is convenient to study in the reference frame co-moving with the absorber. In this vibrating reference frame, the resonant nuclei are at rest while the photon field is phase-modulated. Similar to the recent works [9,10,26,27,33–36], we consider the case of nonrelativistic motion of the absorber. Thus, substituting Equation (6) into Equation (4) results in the following form of the electric field of the incident 14.4 keV single-photon wave packet in the vibrating reference frame:

$$E'_S(\tau_a) = E_0 e^{i\varphi} \theta(\tau_a) e^{-\gamma_S \tau_a - i\omega_{SC} \tau_a + ip \sin(\Omega \tau_a + \vartheta)} \left(e^{i\frac{\Delta}{2} \tau_a - i\delta p \sin(\Omega \tau_a + \vartheta)} - e^{-i\frac{\Delta}{2} \tau_a + i\delta p \sin(\Omega \tau_a + \vartheta)} \right), \quad (7)$$

where $\tau_a = t - z_a/c$, $p = (p_1 + p_2)/2$, and $\delta p = p_2 - p_1$, while $p_1 = \omega_1 R/c$ and $p_2 = \omega_2 R/c$ are the indexes of modulation of the corresponding Lorentzian contours in Equation (1). In Equation (7), we neglected the amplitude modulation of the photon field due to nonrelativistic motion of the absorber (see also [34]). The frequency modulation of the field in Equation (7) due to the Doppler effect is represented in the form of (i) the modulation at the central frequency of the photon wave packet, the amplitude of which is determined by the average modulation index p (the term before brackets in Equation (7)), and (ii) the additional frequency modulation of each Lorentz contour in Equation (1) with amplitude δp (the term inside brackets in Equation (7)). Since $\delta p/p = \Delta/\omega_{SC} \simeq 3 \times 10^{-13}$, one can represent the wave packet Equation (4) at the entrance of the absorber in the vibrating reference frame in the form of the frequency modulated Lorentz-squared single-photon pulse:

$$E'_S(\tau_a) = 2iE_0 e^{i\varphi} \theta(\tau_a) \sin\left(\frac{\Delta}{2} \tau_a\right) e^{-\gamma_S \tau_a - i\omega_{SC} \tau_a + ip \sin(\Omega \tau_a + \vartheta)}, \quad (8)$$

where the reflection of the field from the absorber surface is neglected. Using the Jacobi–Anger expansion, $\exp(ip \sin \alpha) = \sum_{n=-\infty}^{\infty} J_n(p) \exp(in\alpha)$, and taking the Fourier transform of Equation (8), we obtain the spectrum of the SMS photon at the entrance to the resonant absorber in the vibrating reference frame:

$$\begin{aligned} \tilde{E}'_S(\omega) &= \sum_{n=-\infty}^{\infty} J_{-n}(p) e^{-in\vartheta} \tilde{E}_S(\omega - n\Omega) \\ &= \frac{E_0 e^{i\varphi}}{2\pi\gamma_S} \sum_{n=-\infty}^{\infty} J_{-n}(p) e^{-in\vartheta} \left[\frac{1}{1+i(\omega_{SC}-\Delta/2-\omega+n\Omega)/\gamma_S} - \frac{1}{1+i(\omega_{SC}+\Delta/2-\omega+n\Omega)/\gamma_S} \right]. \end{aligned} \quad (9)$$

It can be considered as a superposition of the Lorentz-squared spectral lines of the incident field Equation (1) (see the term in square brackets) with the central frequencies ω_{SC} , separated from each other by the absorber vibration frequency, Ω , with amplitudes determined by the n -th Bessel function of the first kind, depending on the modulation index p , and with phases determined by the initial phase of the absorber vibration, ϑ .

The transformation of each Fourier constituent of the incident field, $\tilde{E}'_S(\omega)$, during its propagation through the vibrating resonant absorber in the vibrating reference frame, is well-known (see [6,7,9,29,33–37] and references therein). It corresponds to the Beer–Lambert–Bouguer law. Assuming that the resonant transition of the ^{57}Fe nucleus has the natural linewidth with half-width $\gamma_a = \Gamma_0/2$, the spectral constituent of the photon field at the exit from the absorber of the thickness, L , can be written in the form:

$$\tilde{E}'_{OUT}(\omega) = \tilde{E}'_S(\omega) \exp\left(-T_e/2 - \frac{T_a/2}{1 + i(\omega_a - \omega)/\gamma_a}\right), \quad (10)$$

where $\tilde{E}'_S(\omega)$ is described by Equation (9), T_e is the exponent factor of photoelectric absorption (the non-resonant optical depth of the absorber), $T_a = f_{LM}\sigma NL$ is the Mössbauer thickness of the absorber resonant transition corresponding to the optical depth of the medium, f_{LM} is the Lamb–Mössbauer factor accounting for the probability of recoilless absorption, σ is the resonant cross-section of the nuclear transition, N is the concentration of ^{57}Fe nuclei in the absorber, and ω_a is the frequency of the nucleus resonant transition. Below, we will consider the stainless-steel foil of a compound Fe:Cr:Ni at 70:19:11 wt.% that is 90% enriched by nuclide ^{57}Fe in iron fraction. In this case, one can consider $T_e \simeq T_a/180$. The inverse Fourier transform of Equation (10), $E'_{OUT}(\tau_a) = \int_{-\infty}^{\infty} \tilde{E}'_{OUT}(\omega) e^{-i\omega\tau_a} d\omega$, determines the temporal form of the single-photon wave packet behind the absorber in the vibrating reference frame. As shown in [9,33–36], the electric field of a single-photon at the exit from the absorber in the laboratory reference frame can be obtained by changing $\tau_a \rightarrow \tau_{lab}$ in $E'_{OUT}(\tau_a)$ and multiplying it by $\exp[-ip \sin(\Omega\tau_{lab} + \vartheta_0)]$. Thus, the time dependence of the intensity of the single-photon wave packet behind the vibrating nuclear absorber is the same in both the vibrating and laboratory reference frames and has the form (more detailed and alternative derivation can be found in [36]):

$$I_{OUT}(t) = \frac{c}{8\pi} |E'_{OUT}(t)|^2 = \frac{I_0 e^{-T_e}}{4\pi^2 \gamma_S^2} \left| \sum_{n=-\infty}^{\infty} J_{-n}(p) e^{-in\vartheta} [E'_{1,n}(t) - E'_{2,n}(t)] \right|^2, \quad (11)$$

where $\tau_a \equiv t$ and $I_0 = cE_0^2/(8\pi)$. The fields $E'_{1,n}(t)$ and $E'_{2,n}(t)$ can be written as

$$E'_{1(2),n}(t) = \int_{-\infty}^{\infty} \frac{1}{1 + i(\omega_{1(2)} + n\Omega - \omega)/\gamma_S} \exp\left[-\frac{T_a/2}{1 + i(\omega_a - \omega)/\gamma_a}\right] e^{-i\omega t} d\omega. \quad (12)$$

According to Equations (11) and (12), the term $[E'_{1,n}(t) - E'_{2,n}(t)]$ characterizes the time dependence of the electric field of the n -th Lorentz-squared spectral line at the exit from the vibrating absorber in the vibrating reference frame, while $E'_{1,n}(t)$ corresponds to the “left” Lorentzian spectral line at the frequency $\omega_1 = \omega_{SC} - \Delta/2$ in Equation (1), and $E'_{2,n}(t)$ corresponds to the “right” spectral line at the frequency $\omega_2 = \omega_{SC} + \Delta/2$.

In contrast to the time dependence of the intensity of the single-photon wave packet at the exit from the vibrating absorber, its spectrum in the laboratory reference frame differs from that in the vibrating reference frame. The output spectrum of the Lorentz-squared single-photon pulse in the laboratory reference frame can be obtained in the same way as in the supplementary material of [33] in the form:

$$\tilde{E}_{OUT}(\omega) = e^{-T_e/2} \sum_{q,n=-\infty}^{\infty} J_{n+q}(p) J_q(p) \tilde{E}_S(\omega - n\Omega) \exp\left\{-\frac{T_a/2}{1 + i[\omega_a + (n+q)\Omega - \omega]/\gamma_a}\right\}. \quad (13)$$

In the next sections, based on Equations (11) and (12), we will analyze the possibility of transforming the incident 14.4 keV Lorentz-squared single-photon wave packets, Equations (1) and (4), into a regular sequence of an arbitrary number of short, nearly bandwidth-limited pulses, including a single short pulse via its transmission through the vibrating ^{57}Fe resonant absorber.

3. Formation of Ultrashort Pulse Train

The basic method of formation of the ultrashort pulse train from the quasi-monochromatic single-photon wave packet of SMS (Equations (1) and (4)) is the same as the method proposed in [26,27], implemented in [9,10], and discussed in detail in [34,35] for the Lorentzian single-photon pulse. The method is based on the transmission of the single-photon pulse through the resonant frequency tuned absorber vibrating along the photon propagation direction. The physical mechanism of the pulse formation is most clear when the vibration frequency significantly exceeds the source linewidth, $\Omega/\gamma_S \gg 1$. In this case, the spectrum of the incident field in the vibrating reference frame is a set of well-separated Lorentz-squared spectral lines (Figure 2) corresponding to Equation (9). As can be seen in Figure 2, for $p = 1.84$ all lines are phase-aligned, except two lines with indexes $n = -1$ and $n = -3$ in Equation (9), which are antiphase to the others. The destructive interference of these spectral lines compensates for the constructive interference of other lines, so that any amplitude modulation of the incident field in the vibrating reference frame is absent. There is only the phase modulation. Even if only one of these lines is removed, the amplitude–phase balance between them will be destroyed and the amplitude modulation in the photon waveform will appear due to constructive interference of the remaining lines. The case of removing one antiphase line from the spectrum of the Lorentzian single-photon pulse was implemented in [9,10] via tuning the line to be removed into resonance with the absorber spectral line. The case of removing all antiphase spectral lines of significant intensity from the Lorentzian single-photon wave packet was discussed in [37].

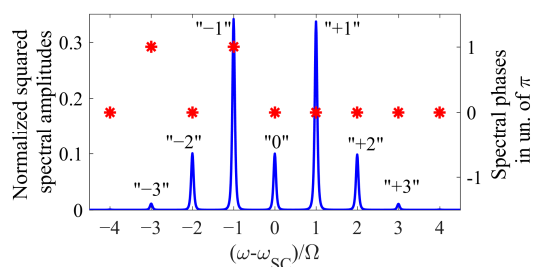


Figure 2. Normalized squared spectral amplitudes (left axis, blue line) and spectral phases at peaks of the squared spectral amplitude (right axis, red stars) (see Equation (9)) of the 14.4 keV Lorentz-squared single-photon wave packet in the vibrating reference frame at $p = 1.84$, $\Omega/\gamma_a = 90$ ($\Omega/(2\pi) \approx 51$ MHz), and $\vartheta = 0$. The “−1” spectral line will be removed at the exit from the optically thick absorber. The spectrum normalization is the same as for the red solid curve in Figure 1a.

Consider the case of removing the minus first line from the spectrum of the Lorentz-squared single-photon wave packet. If the absorber vibrates with amplitude $R \simeq 0.25\text{\AA}$, corresponding to the modulation index $p \simeq 1.84$, the first plus and minus Lorentz-squared spectral lines of the incident field in the vibrating reference frame (Equation (9) and Figure 2) take the maximum value due to maximization of $J_{\pm 1}^2(1.84)$. Therefore, the resonant suppression of the minus first spectral line will lead to maximum destruction of the amplitude–phase balance in the spectrum of the transmitted field and, hence, to maximum amplitude modulation in the photon waveform behind the absorber. As implemented in [9] for the Lorentzian photons, in this case, the amplitude modulation takes the form of a regular sequence of short nearly bandwidth-limited pulses with pulse duration determined by the full width of the spectrum in the vibrating reference frame and with the repetition rate of Ω .

Let us analytically find the conditions for the formation of the most intense short pulses from the SMS Lorentz-squared single-photon wave packet when the vibration frequency is high enough, i.e., $\Omega/\gamma_S \gg 1$. In this case, only the minus first spectral line is resonantly absorbed by the absorber. This allows one to separate the terms in Equation (11) into two parts. The first part includes all non-resonant spectral lines with $n \neq -1$. For this group, Equation (12) can be represented in the form of Equation (A10) (see Appendix A). As follows from Equation (A10), the interaction of the non-resonant spectral lines with the absorber can be neglected if

$$\frac{T_a \gamma_a}{2\Omega} \ll 1. \quad (14)$$

Assuming the validity of the condition Equation (14), one can write for all $n \neq -1$:

$$E'_{1,n}(t) - E'_{2,n}(t) \simeq 4\pi i \gamma_S \theta(t) \sin\left(\frac{\Delta}{2}t\right) e^{-i(\omega_{SC} + n\Omega)t - \gamma_S t}. \quad (15)$$

The second part includes the Lorentz-squared spectral line with $n = -1$ resonant to the absorber quantum transition. This term in Equation (12) can be represented in the form of Equation (A9) (see Appendix A):

$$E'_{1,-1}(t) - E'_{2,-1}(t) = 2\pi \gamma_S \theta(t) e^{-i\omega_a t - \gamma_a t} \sum_{k=0}^{\infty} \left\{ \left[\frac{i\Delta/2 - (\gamma_S - \gamma_a)}{T_a \gamma_a / 2} \right]^k - \left[\frac{-i\Delta/2 - (\gamma_S - \gamma_a)}{T_a \gamma_a / 2} \right]^k \right\} \left(\frac{T_a \gamma_a t}{2} \right)^{\frac{k}{2}} J_k \left(2\sqrt{\frac{T_a \gamma_a}{2}} t \right). \quad (16)$$

As follows from Equation (16), the term with $k = 0$ equals zero. Other terms in the sum of Equation (16) can be neglected, except for the term with $k = 1$, if:

$$\frac{\sqrt{(\Delta/2)^2 + (\gamma_S - \gamma_a)^2}}{T_a \gamma_a / 2} \ll 1 \quad (17)$$

Under the considered parameter values of the absorber and the incident field, namely, $\gamma_S = 2.35\Gamma_0$, $\gamma_a = 0.5\Gamma_0$, and $\Delta = 0.94\Gamma_0$, the inequality (17) determines the minimum Mössbauer thickness of the absorber, namely, $T_a \gg 7.6$. In this case, the amplitude of the resonant spectral component with $n = -1$ has the form:

$$E'_{1,-1}(t) - E'_{2,-1}(t) \simeq 4\pi i \gamma_S \theta(t) e^{-i(\omega_{SC} - \Omega)t - \gamma_a t} \frac{\Delta}{T_a \gamma_a} \sqrt{\frac{T_a \gamma_a t}{2}} J_1 \left(2\sqrt{\frac{T_a \gamma_a}{2}} t \right), \quad (18)$$

where we have considered that $\omega_a = \omega_{SC} - \Omega$. Substituting Equations (15) and (18) into Equation (11), we can obtain an analytical solution for the 14.4 keV SMS Lorentz-squared photon waveform:

$$I_{OUT}^{(analyt)}(t) = 4I_0 \theta(t) e^{-2\gamma_S t - T_e} \left| \sin\left(\frac{\Delta}{2}t\right) e^{ip \sin(\Omega t + \vartheta)} + J_1(p) A_{FS}(t) e^{i(\Omega t + \vartheta)} \right|^2, \quad (19)$$

where,

$$A_{FS}(t) \equiv |A_{FS}(t)| \exp[i\Phi_{FS}(t)] = \frac{\Delta}{T_a \gamma_a} e^{(\gamma_S - \gamma_a)t} \left(\sqrt{T_a \gamma_a t / 2} \right) J_1 \left(2\sqrt{T_a \gamma_a t / 2} \right) - \sin\left(\frac{\Delta}{2}t\right). \quad (20)$$

According to Equation (19), the radiation at the exit from the vibrating resonant absorber can be represented as the interference of the incident field (the first term inside the modulus), which in the vibrating reference frame is phase-modulated, and the coherently scattered field (the second term inside the modulus) at the central frequency of the removed minus first spectral line (with amplitude proportional to $J_1(p)$). The time dependence of the coherently scattered field is determined by Equation (20). As discussed above, the

modulation index $p \simeq 1.84$ corresponds to the absolute maximum of the first-order Bessel function. Therefore, at this value, the amplitude of the coherently scattered field is the maximum. According to Equation (19), the time moments of formation of pulse peaks, t_{pulse} , are determined by the condition that the phase difference between the incident and coherently scattered fields is $2\pi n$, $n \in \mathbb{Z}$:

$$\Omega t_{pulse} + \vartheta + \Phi_{FS}(t_{pulse}) - p \sin(\Omega t_{pulse} + \vartheta) - \Phi_{input}(t_{pulse}) = 2\pi n, \quad (21)$$

where $\Phi_{input}(t)$ is an addition to the phase of the incident field due to sign reversal of the function $\sin(\frac{\Delta}{2}t)$. Since the amplitudes of the incident and coherently scattered fields, i.e., $\sin(\frac{\Delta}{2}t)$ and $A_{FS}(t)$, are the real functions of time, the phases $\Phi_{FS}(t_{pulse})$ and $\Phi_{input}(t_{pulse})$ represent only a change in the sign of the slowly varying (compared to Ω) amplitudes of the corresponding fields. Thus, according to Equation (21), the times of pulse formation are determined by $\Omega t_{pulse} + \vartheta$. Therefore, the change in the initial vibration phase of the absorber, ϑ , leads to the time shift of the pulses within one vibration period of the absorber, while the pulse repetition period is equal to the absorber vibration period. As a result, at a high vibration frequency, a regular train of short pulses with high repetition rates is formed. The pulse peaks form the envelope, which is obtained by substituting Equation (21) into Equation (19):

$$I_{OUT}^{(analyt)}(t_{pulse}) \equiv I_{peak} = 4I_0 \theta(t_{pulse}) e^{-2\gamma_S t_{pulse} - T_e} \left[\left| \sin\left(\frac{\Delta}{2}t_{pulse}\right) \right| + \left| J_1(p) A_{FS}(t_{pulse}) \right| \right]^2. \quad (22)$$

As can be seen from Equation (22), at the above parameter values of the incident field and the vibrating absorber, the envelope of the pulse train as a function of the moments, t_{pulse} , is determined by the resonant Mössbauer thickness of the absorber, T_a (Figure 3). One can see that at $15 \leq T_a \leq 150$, the peak intensity of the produced pulses can be higher than the peak intensity of the incident single-photon wave packet. The corresponding time interval is determined by T_a . For example, at $T_a = 15$, this time interval is $50 \text{ ns} < t_{pulse} < 110 \text{ ns}$, while at $T_a = 150$ — $39 \text{ ns} < t_{pulse} < 57 \text{ ns}$. The pulses with the highest intensity, which exceeds the peak intensity of the incident single-photon wave packet by 2.34 times, are formed in the vibrating absorber with $T_a = 44$ in the vicinity of $t_{pulse} = 72 \text{ ns}$. This optical depth satisfies the condition Equation (17), while for applicability of the analytical solution, Equation (14), the oscillation frequency of the absorber should be $\Omega/(2\pi) \gg 12.4 \text{ MHz}$.

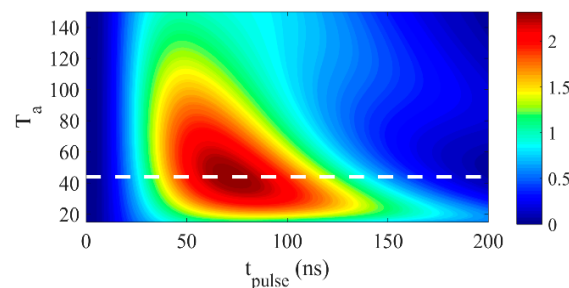


Figure 3. Dependence of I_{peak} on the optical thickness, T_a , and time, t_{pulse} , according to Equations (20) and (22) at $p = 1.84$, $\gamma_S = 2.35\Gamma_0$, $\gamma_a = 0.5\Gamma_0$, $\Delta = 0.94\Gamma_0$, and $T_e = T_a/180$. The white dashed line corresponds to $T_a = 44$, at which the peak pulse intensity is the maximum at the moment $t_{pulse} = 72 \text{ ns}$ and is 2.34 times higher than the peak intensity of the incident photon. Here, I_{peak} is normalized to the peak intensity of the incident photon wave packet.

In Figure 4a, we show the time dependence of the intensity of the 14.4 keV SMS Lorentz-squared single-photon wave packet at the exit from the resonant ^{57}Fe absorber with the optimal Mössbauer thickness, $T_a = 44$, vibrating at frequency $\Omega/(2\pi) \approx 51 \text{ MHz}$

$(\Omega/\gamma_a = 90)$, with the amplitude $R \simeq 0.25\text{\AA}$ corresponding to the modulation index $p = 1.84$. At the considered vibration frequency, the FWHM pulse duration is 3.6 ns, while the repetition period is 19.7 ns. A good agreement is seen between the curve, based on the analytical solution in Equations (19) and (20) (blue dotted line), and the curve, showing the numerical integration of the accurate solution in Equations (11) and (12) (red solid line). The slight difference between the numerical and analytical solutions is mainly due to the neglect of terms with powers of $k > 1$ in Equation (16).

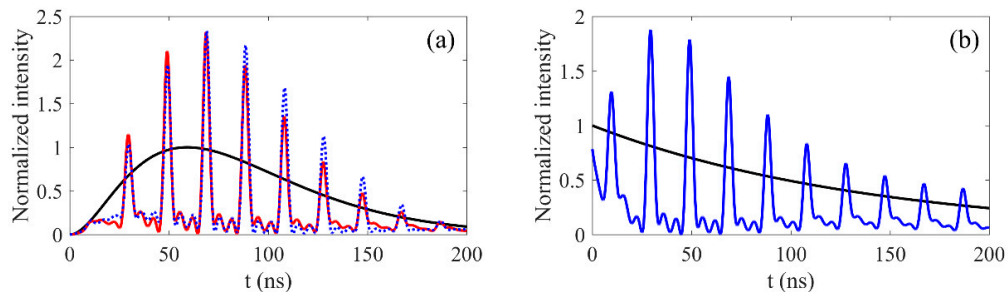


Figure 4. (a) Time dependence of the intensity of the 14.4 keV SMS Lorentz-squared single-photon wave packet ($\gamma_S = 2.35\Gamma_0$ and $\Delta = 0.94\Gamma_0$) at the exit from the resonant ^{57}Fe absorber with $T_a = 44$, $T_e = T_a/180$, and $\gamma_a = 0.5\Gamma_0$, which harmonically oscillates at the frequency $\Omega/\gamma_a = 90$ ($\Omega/(2\pi) \approx 51$ MHz) with the amplitude $R \approx 0.25\text{\AA}$ ($p = 1.84$) and the initial vibration phase $\vartheta = 0$. The red solid curve corresponds to the numerical integration of Equations (11) and (12), the blue dotted curve corresponds to the analytical solution in Equations (19) and (20), while the black solid curve shows the photon waveform at the entrance to the absorber. Here, the intensity is normalized to the peak intensity at the entrance to the medium. (b) Time dependence of the intensity of the 14.4 keV Lorentzian single-photon wave packet ($\gamma_S = 0.5\Gamma_0$) at the exit from the same vibrating resonant ^{57}Fe absorber plotted according to [34]. The intensity is normalized to the peak intensity of the Lorentzian single-photon wave packet at the entrance to the medium.

As can be seen from the comparison of Figure 4a,b, the absence of the stepwise front edge of the Lorentz-squared single-photon pulse leads to the absence of the Sommerfeld–Brillouin precursor in the output waveform and to a qualitative difference in the produced pulse sequence. The pulse sequence produced from the Lorentz-squared single-photon wave packet is more similar to pulses used in laser quantum optics and more suitable for potential applications.

As shown in Figure 4a, the total duration of the produced pulse sequence is determined by the duration of the incident single-photon wave packet. The pulse repetition period is equal to the period of the absorber vibration. A decrease or increase in the absorber vibration period at a fixed vibration amplitude, $R \simeq 0.25\text{\AA}$, results in a proportional shortening or lengthening of both the pulse duration and the repetition period, leading to an increase or decrease, respectively, in the number of pulses in the sequence. Thus, the absorber vibration frequency controls the number of significant pulses in the produced sequence. At the available vibration frequency up to 24 GHz [38], the produced pulses can have a duration down to 10 ps, corresponding to formation of more than 10^4 significant pulses. On the other hand, if the period of the absorber vibration is comparable to the duration of the incident single-photon wave packet, then only several short pulses can be produced. In this case, the produced short pulses, except for one, can appear in low-intensity regions of either the front edge or the tail of the photon waveform and, therefore, can be much weaker than one of the pulses. This corresponds to the compression of the incident long Lorentz-squared single-photon pulse into a short single pulse and is possible owing to a gradual increase in the front edge and the absence of the Sommerfeld–Brillouin precursor.

4. Compression of the Lorentz-Squared Single-Photon Pulse

Let us consider the conditions for compression of the 14.4 keV Lorentz-squared single-photon pulse into a relatively intense and short single pulse in the vibrating ^{57}Fe

resonant absorber. Since a low vibration frequency is required in this case, the analytical solution in Equations (19) and (20) becomes unsuitable, and the general solution in Equations (11) and (12) should be numerically analyzed.

The condition for the formation of a single intense pulse in the photon waveform implies a maximum in its peak intensity and a minimum in the intensity of adjacent pulses within the waveform. This condition can be searched as the maximum value of the function:

$$\Delta I = \left(I_{OUT}^{(\max 1)} - I_{OUT}^{(\max 2)} \right) / I_{INPUT}^{(\max)}, \quad (23)$$

where $I_{OUT}^{(\max 1)}$ and $I_{OUT}^{(\max 2)}$ are the peak intensities of the two most intense pulses within the single-photon waveform ($I_{OUT}^{(\max 1)} > I_{OUT}^{(\max 2)}$) normalized to the peak intensity of the incident photon wave packet, $I_{INPUT}^{(\max)}$. Maximization of ΔI means the formation of an intense and short single nearly bandwidth-limited pulse.

Let us consider ΔI using Equations (11) and (12) under the above parameter values as a function of three variables: the resonant Mössbauer thickness of the absorber, T_a , the absorber vibration frequency, Ω , and the initial phase of the absorber vibration, ϑ , locked to the front edge of the single-photon waveform.

First, we fix some Mössbauer thickness of the absorber, T_a . Figure 5a represents 2D dependence of the function ΔI on the frequency of the absorber vibration, Ω , and the initial vibration phase, ϑ , at $T_a = 21$. As can be seen in Figure 5a, if the vibration frequency is high, the value of ΔI is small, whereas the dependence of ΔI on ϑ is weak. This is because the repetition period of the short pulses in a sequence is small, so that the two most intense pulses (the red line in Figure 4a) are formed near the maximum of the incident photon waveform (black line in Figure 4a) and have a comparable intensity. As discussed above, variation of ϑ causes the time shift of the produced short pulses within one period of the absorber vibration. In a small vibration period (high Ω), this shift relative to the envelop of the incident single-photon wave packet (black line in Figure 4a) is also small, which results in a weak dependence of ΔI on ϑ .

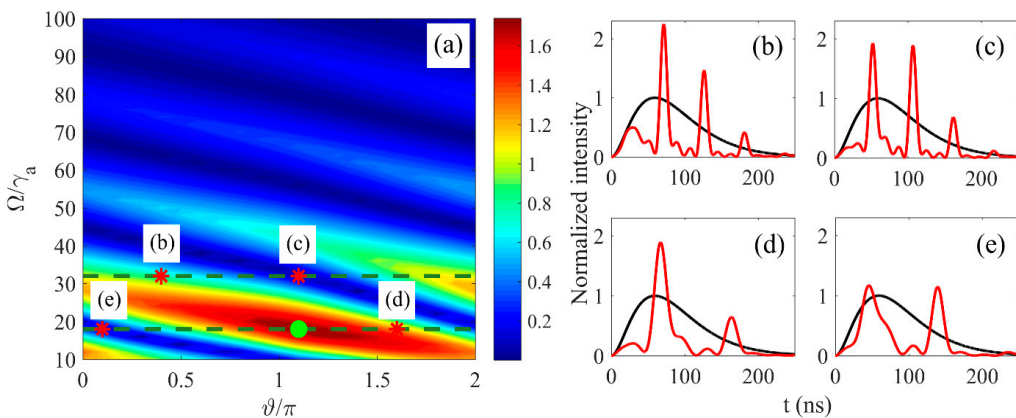


Figure 5. (a) Dependence of the function ΔI (according to (23)) for the Lorentz-squared single-photon pulse at the exit from the ^{57}Fe absorber ($\gamma_a = 0.5\Gamma_0$) with $T_a = 21$, harmonically vibrating with amplitude $R \approx 0.25 \text{ \AA}$ ($p = 1.84$), frequency Ω , and the initial phase ϑ . The spectral-temporal properties of the incident field correspond to Equations (1) and (4), with $\gamma_S = 2.35\Gamma_0$ and $\Delta = 0.94\Gamma_0$. The non-resonant optical thickness is $T_e = T_a/180$. The upper and lower dashed horizontal lines mark the absorber vibration period, $2\pi/\Omega = 55.4 \text{ ns}$ ($\Omega/\gamma_a = 32$) and 98.4 ns ($\Omega/\gamma_a = 18$), respectively. Stars mark $\vartheta = 0.4\pi$ and $\Omega/\gamma_a = 32$ for (b), $\vartheta = 1.1\pi$ and $\Omega/\gamma_a = 32$ for (c), $\vartheta = 1.6\pi$ and $\Omega/\gamma_a = 18$ for (d), and $\vartheta = 0.1\pi$ and $\Omega/\gamma_a = 18$ for (e). The green circle marks the maximum value of $\Delta I \equiv \Delta I_{opt} \approx 1.76$ achieved at $\Omega_{opt}/\gamma_a \approx 18$ and $\vartheta_{opt} \approx 1.1\pi$. In panels (b–e) red and black curves show the time dependences of the intensity of the 14.4 keV SMS Lorentz-squared single-photon wave packet at the exit from and entrance to the medium, respectively.

At low vibration period comparable to the duration of the incident single-photon wave packet, $2\pi/\Omega \sim 100$ ns, only several short pulses are formed at the exit from the absorber (Figure 5b–e). Therefore, (i) the difference between the peak pulse intensities, ΔI , becomes larger, and (ii) the dependence of ΔI on ϑ becomes much stronger. Both take place since the formed short pulses are separated by a large interval comparable to the duration of the incident wave packet. As shown in Figure 5b–e, in this case, one can control the relative amplitudes of the produced short pulses via change of the initial phase of the absorber vibration, ϑ . For $T_a = 21$ and other parameter values in Figure 5, the maximum of ΔI is achieved at $\Omega_{opt}(T_a = 21)/\gamma_a \simeq 18$ and $\vartheta_{opt}(T_a = 21) \simeq 1.1\pi$. It is $\Delta I_{opt}(T_a = 21) \equiv \max\{\Delta I(T_a = 21)\} \simeq 1.76$ (green circle in Figure 5a).

Further, to find the Mössbauer thickness, T_a^* , providing the absolute maximum value of ΔI marked as $\Delta I_{max} \equiv \max\{\Delta I_{opt}(T_a)\} \equiv \Delta I(T_a^*, \Omega_{opt}^*, \vartheta_{opt}^*)$, we plotted 2D dependences of ΔI on Ω and ϑ for various values of T_a similar to Figure 5a. Then, for each value of T_a , we determined $\Delta I_{opt}(T_a)$ achieved at $\Omega_{opt}(T_a)$ and $\vartheta_{opt}(T_a)$. The obtained set of dependences is shown in Figure 6. Finally, from this set, the absolute maximum, $\Delta I_{max} \simeq 1.76$, together with the corresponding values of $\Omega_{opt}^*/\gamma_a \simeq 18$ and $\vartheta_{opt}^* \simeq 1.1\pi$ achieved at $T_a^* \simeq 21$, was determined (Figure 6). These optimum values correspond to the vibration frequency $\Omega_{opt}^*/(2\pi) \simeq 10.2$ MHz, the physical thickness of the considered stainless-steel foil of about 2.1 μ m, and the time delay of the moment of emission of 14.4 keV photons from the synchrotron storage ring relative to the zero absorber's vibration phase of about 54 ns.

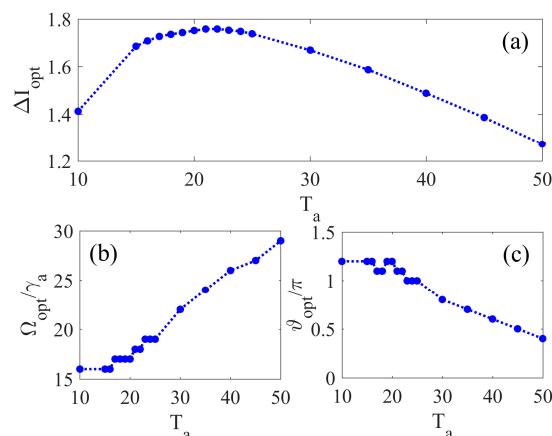


Figure 6. Dependence of ΔI_{opt} (a), as well as the corresponding dependence of Ω_{opt}/γ_a (b) and ϑ_{opt}/π (c) on the absorber Mössbauer thickness, T_a . Maximum of $\Delta I_{opt}(T_a)$ is achieved at $T_a = T_a^* \simeq 21$. At this value, $\Omega_{opt}(T_a^*)/\gamma_a \equiv \Omega_{opt}^*/\gamma_a \simeq 18$, and $\vartheta_{opt}(T_a^*) \equiv \vartheta_{opt}^* \simeq 1.1\pi$.

The intensity and spectrum of the Lorentz-squared single-photon wave packet transmitted through the ^{57}Fe absorber in this case is shown in Figure 7. The transmitted photon waveform consists of one high-intensity bell-shaped short pulse, both preceded and followed by weak bursts, the highest of which is 7 times smaller than the high-intensity pulse. This can be interpreted as the compression of the incident single-photon pulse. The peak intensity of the compressed pulse is 2.1 times higher than the peak intensity of the incident single-photon pulse. The duration of the output high-intensity short pulse is 18.2 ns, which corresponds to 5.5-fold compression of the incident single-photon wave packet. The spectrum of the output field in the laboratory reference frame, $|\tilde{E}_{OUT}(\omega)|^2$, plotted using Equation (13), has an effective width of 2.4 Ω , which exceeds the width of the incident field spectrum by more than six times (black line in Figure 7b).

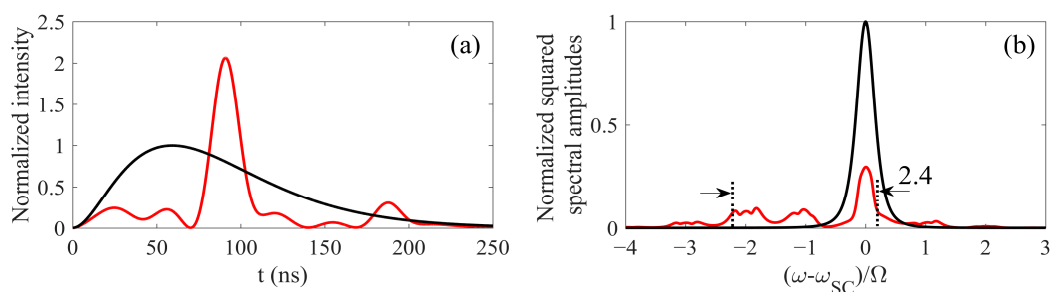


Figure 7. (a) Time dependence of the intensity of the 14.4 keV Lorentz-squared single-photon wave packet (4) with $\gamma_S = 2.35\Gamma_0$ and $\Delta = 0.94\Gamma_0$ at the entrance of (black line) and exit from (red line) the resonant ^{57}Fe absorber with $T_a = 21$, $T_e = T_a/180$, and $\gamma_a = 0.5\Gamma_0$, which harmonically vibrates at frequency $\Omega/\gamma_a = 18$ ($\Omega/(2\pi) \approx 10.2$ MHz) with amplitude $R \approx 0.25$ Å ($p = 1.84$) and initial vibration phase $\vartheta = 1.1\pi$. The intensity is normalized to the peak intensity at the entrance to the medium. (b) The corresponding normalized squared spectral amplitude of the single-photon field in the laboratory reference frame at the exit from the vibrating resonant absorber, $|\tilde{E}_{OUT}(\omega)|^2$ (according to Equation (13), red curve), and at the entrance to the vibrating resonant absorber, $|\tilde{E}_S(\omega)|^2$ (according to Equation (1), black curve).

As can be seen from Figure 6, compression of the ESRF SMS Lorentz-squared single-photon pulse into a single bell-shaped short pulse, similar to the pulse shown in Figure 7, can be obtained not only under the above-determined parameter values. About a two-fold increasing peak intensity and five-fold shortening the ESRF SMS Lorentz-squared single-photon pulse can be implemented with ^{57}Fe stainless-steel foil, having the Mössbauer thickness $15 \leq T_a \leq 25$, the vibration frequency $16 \leq \Omega_{opt}/\gamma_a \leq 19$ (9 MHz $\leq \Omega_{opt}/(2\pi) \leq 10.7$ MHz), and the initial vibration phase $\pi \leq \vartheta_{opt} \leq 1.2\pi$. These conditions are similar to the conditions realized in [9] for the case of a ^{57}Co source, and hence can be readily implemented in the case of SMS.

5. Conclusions

In this paper, we have shown the possibility and proposed an experiment for transforming the waveform of a 14.4 keV photon (time dependence of the photon detection probability or, equivalently, the intensity of the single-photon wave packet) emitted by a synchrotron Mössbauer source (SMS) into a regular sequence of short nearly bandwidth-limited pulses with a controlled number of pulses in an oscillating recoilless ^{57}Fe resonant absorber. The case of the single-photon wave packet with a Lorentz-squared spectrum produced by SMS at the European Synchrotron Radiation Facility (ESRF) was discussed. The main feature of this single-photon pulse is a smooth front edge of the intensity, in contrast to the stepwise front edge of 14.4 keV single-photon wave packet with the Lorentz spectrum emitted by the ^{57}Co radioactive Mössbauer source. As a result, a waveform of the Lorentz-squared photon transmitted through a resonant medium does not contain the Sommerfeld–Brillouin precursor (a part of the photon waveform containing the front edge that is not changed in the medium). This opens the possibility of compressing the waveform of SMS photons into a single short pulse, which is impossible with the Lorentzian photons.

The proposed method is similar to the method implemented in the proof-of-principle experiments with photons emitted by a ^{57}Co source, where the Lorentzian single-photon pulse with a stepwise front edge was transformed into various regular sequences of short pulses [9,10]. The method is based on the transmission of the SMS photons through a piston-like vibrating stainless-steel foil enriched with ^{57}Fe nuclide. However, in contrast to the case of the ^{57}Co source, the initial phase of the absorber vibration can be locked to the front edge of the single-photon wave packet if the absorber vibration frequency is a multiple of the synchrotron pulse repetition rate. This makes it possible to produce a specific single-photon wave packet with a controlled waveform, suitable for applications in X-ray quantum optics, in particular for implementation of quantum nuclear memory,

i.e., storage of the single X-ray photon in a nuclear coherence of an ensemble of nuclei and its retrieval on demand [25].

We have proposed the experimentally available conditions for compression of a 100 ns-length 14.4 keV single-photon wave packet produced by SMS at the ESRF into a single bell-shaped pulse of less than 20 ns duration and more than twice the peak intensity. These conditions can be satisfied in a relatively wide region of the parameter values. On demand, one can also obtain two, three, or several pulses, for which the relative peak intensities can be varied by changing the initial phase of the absorber vibration.

Such single-photon coherent pulses are promising for applications in the field of X-ray quantum optics, including the potential implementation of quantum memory and quantum information processing.

Author Contributions: Conceptualization, I.R.K., Y.V.R. and O.K.; investigation, I.R.K. and Y.V.R.; software, I.R.K.; supervision, Y.V.R.; visualization, I.R.K. and Y.V.R.; writing—original draft, I.R.K. and Y.V.R.; writing—review and editing, I.R.K., Y.V.R. and O.K. All authors have read and agreed to the published version of the manuscript.

Funding: The research was supported by the Center of Excellence “Center of Photonics”, funded by the Ministry of Science and Higher Education of the Russian Federation under Contract No. 075-15-2022-316. O.K. acknowledges support from the National Science Foundation (NSF, Grant No. PHY-2012194). I.R.K. acknowledges personal support from the Foundation for the Advancement of Theoretical Physics and Mathematics “BASIS”.

Data Availability Statement: Data sharing is not applicable to this article.

Conflicts of Interest: The authors declare no conflict of interest.

Appendix A

Let us calculate the integral Equation (12) using the theory of residues. Similar calculations were performed in [5,39]. First, let us rewrite Equation (12) in the equivalent form:

$$E'_{1(2),n}(t) = 2\pi\gamma_S \cdot \frac{1}{2\pi i} \int_{-\infty}^{\infty} \frac{1}{\omega + \omega_{1(2)} + n\Omega - i\gamma_S} \exp\left[\frac{iT_a\gamma_a/2}{\omega + \omega_a - i\gamma_a}\right] e^{i\omega t} d\omega. \quad (\text{A1})$$

The expression under the integral has two poles on the complex plane: $-(\omega_{1(2)} + n\Omega) + i\gamma_S$ and $-\omega_a + i\gamma_a$. Thus, $E'_{1(2),n}(t)$ can be represented as the sum of two contour integrals around the singular points:

$$E'_{1(2),n}(t) = 2\pi\gamma_S \cdot \left[\frac{1}{2\pi i} \oint_{-(\omega_{1(2)}+n\Omega)+i\gamma_S} Q d\omega + \frac{1}{2\pi i} \oint_{-\omega_a+i\gamma_a} Q d\omega \right], \quad (\text{A2})$$

where $Q = \frac{1}{\omega + \omega_{1(2)} + n\Omega - i\gamma_S} \exp\left[\frac{iT_a\gamma_a/2}{\omega + \omega_a - i\gamma_a}\right] e^{i\omega t}$. Let us start with the first contour integral. Making the change of variables $z = \omega + \omega_{1(2)} + n\Omega - i\gamma_S$, it is easy to show that:

$$\frac{1}{2\pi i} \oint_{-(\omega_{1(2)}+n\Omega)+i\gamma_S} Q d\omega = \theta(t) e^{-i(\omega_{1(2)}+n\Omega)t - \gamma_S t} \exp\left[\frac{iT_a\gamma_a/2}{\omega_a - \omega_{1(2)} - n\Omega + i(\gamma_S - \gamma_a)}\right]. \quad (\text{A3})$$

Using the formula for generating Bessel functions, $\exp[x(u - 1/u)/2] = \sum_{n=-\infty}^{\infty} u^m J_m(x)$, Equation (A3) can be rewritten as:

$$\frac{1}{2\pi i} \oint_{-(\omega_{1(2)}+n\Omega)+i\gamma_S} Qd\omega = \theta(t)e^{-i\omega_a t - \gamma_a t} \sum_{k=-\infty}^{\infty} \left[\frac{iT_a \gamma_a / 2}{\omega_a - \omega_{1(2)} - n\Omega + i(\gamma_S - \gamma_a)} \right]^k \left(\frac{T_a \gamma_a t}{2} \right)^{-\frac{k}{2}} J_k \left(2\sqrt{\frac{T_a \gamma_a}{2}} t \right). \quad (\text{A4})$$

Next, we turn to the calculation of the second contour integral in Equation (A2). Let us make a change $z = \omega + \omega_a - i\gamma_a$ and rewrite it in the form:

$$\frac{1}{2\pi i} \oint_{-\omega_a+i\gamma_a} Qd\omega = \frac{1}{2\pi i} e^{-i\omega_a t - \gamma_a t} \oint_{z=0} \frac{dz}{z + \omega_{1(2)} - \omega_a + n\Omega - i(\gamma_S - \gamma_a)} \exp \left[i \left(tz + \frac{T_a \gamma_a / 2}{z} \right) \right]. \quad (\text{A5})$$

Further, we expand the functions under the integral in a Laurent series in the vicinity of the singular point $z = 0$:

$$\frac{1}{z + \omega_{1(2)} - \omega_a + n\Omega - i(\gamma_S - \gamma_a)} = - \sum_{k=0}^{\infty} \frac{z^k}{[\omega_a - \omega_{1(2)} - n\Omega + i(\gamma_S - \gamma_a)]^{k+1}}, \quad (\text{A6})$$

$$\exp \left[i \left(tz + \frac{T_a \gamma_a / 2}{z} \right) \right] = \sum_{m=-\infty}^{\infty} i^m \left(\frac{t}{T_a \gamma_a / 2} \right)^{m/2} z^m J_m \left(2\sqrt{T_a \gamma_a t / 2} \right). \quad (\text{A7})$$

Substituting Equations (A6) and (A7) in Equation (A5) and considering that the value of the integral is proportional to the factor corresponding to z^{-1} in the expansion of the integrand in Equation (A5), we obtain:

$$\frac{1}{2\pi i} \oint_{-\omega_a+i\gamma_a} Qd\omega = -\theta(t)e^{-i\omega_a t - \gamma_a t} \sum_{k=1}^{\infty} \left[\frac{iT_a \gamma_a / 2}{\omega_a - \omega_{1(2)} - n\Omega + i(\gamma_S - \gamma_a)} \right]^k \left(\frac{T_a \gamma_a t}{2} \right)^{-\frac{k}{2}} J_k \left(2\sqrt{\frac{T_a \gamma_a}{2}} t \right). \quad (\text{A8})$$

Thus, by substituting Equations (A3) and (A8) or Equations (A4) and (A2), one can write two equivalent expressions for $\tilde{E}'_{1(2),n}(t)$:

$$E'_{1(2),n}(t) = 2\pi\gamma_S \theta(t) e^{-i\omega_a t - \gamma_a t} \sum_{k=0}^{\infty} \left[\frac{i(\omega_a - \omega_{1(2)} - n\Omega + i(\gamma_S - \gamma_a))}{T_a \gamma_a / 2} \right]^k \left(\frac{T_a \gamma_a t}{2} \right)^{\frac{k}{2}} J_k \left(2\sqrt{\frac{T_a \gamma_a}{2}} t \right), \quad (\text{A9})$$

$$E'_{1(2),n}(t) = 2\pi\gamma_S \theta(t) \left\{ e^{-i(\omega_{1(2)}+n\Omega)t - \gamma_S t} \exp \left[\frac{iT_a \gamma_a / 2}{\omega_a - \omega_{1(2)} - n\Omega + i(\gamma_S - \gamma_a)} \right] - e^{-i\omega_a t - \gamma_a t} \sum_{k=1}^{\infty} \left[\frac{iT_a \gamma_a / 2}{\omega_a - \omega_{1(2)} - n\Omega + i(\gamma_S - \gamma_a)} \right]^k \left(\frac{T_a \gamma_a t}{2} \right)^{-\frac{k}{2}} J_k \left(2\sqrt{\frac{T_a \gamma_a}{2}} t \right) \right\}. \quad (\text{A10})$$

As can be seen, Equation (A9) is convenient to use at a small absolute value of $i[\omega_a - \omega_{1(2)} - n\Omega + i(\gamma_S - \gamma_a)] / (T_a \gamma_a / 2)$, or Equation (A10) otherwise.

References

- Adams, B.W.; Butch, C.; Cavaletto, S.M.; Evers, J.; Harman, Z.; Keitel, C.H.; Palffy, A.; Picon, A.; Röhlsberger, R.; Rostovtsev, Y.; et al. X-ray quantum optics. *J. Mod. Opt.* **2013**, *60*, 2–21. [[CrossRef](#)]
- Hau-Riege, S.P. *Nonrelativistic Quantum X-ray Physics*; Wiley-VCH Verlag GmbH & Co. KGaA: Weinheim, Germany, 2015.
- Röhlsberger, R.; Evers, J.; Shwartz, S. Quantum and nonlinear optics with hard X-rays. In *Synchrotron Light Sources and Free-Electron Lasers*; Jaeschke, E., Khan, S., Schneider, J., Hastings, J., Eds.; Springer Nature Switzerland AG: Cham, Switzerland, 2020; pp. 1399–1431.
- Yoshida, Y.; Langouche, G. (Eds.) *Mössbauer Spectroscopy: Tutorial Book*; Springer: Berlin/Heidelberg, Germany, 2013.
- Lynch, F.J.; Holland, R.E.; Hamermesh, M. Time dependence of resonantly filtered gamma rays from Fe57. *Phys. Rev.* **1960**, *120*, 513–520. [[CrossRef](#)]

6. Smirnov, G.V. General properties of nuclear resonant scattering. *Hyperfine Interact.* **1999**, *123*, 31–77. [[CrossRef](#)]
7. Ikonen, E.; Helistö, P.; Katila, T.; Riski, K. Coherent transient effects due to phase modulation of recoilless γ radiation. *Phys. Rev. A* **1985**, *32*, 2298. [[CrossRef](#)]
8. Helistö, P.; Tittonen, I.; Lippmaa, M.; Katila, T. Gamma Echo. *Phys. Rev. Lett.* **1991**, *66*, 2037. [[CrossRef](#)]
9. Vagizov, F.; Antonov, V.; Radeonychev, Y.V.; Shakhmuratov, R.N.; Kocharovskaya, O. Coherent control of the waveforms of recoilless γ -photons. *Nature* **2014**, *508*, 80. [[CrossRef](#)]
10. Shakhmuratov, R.N.; Vagizov, F.G.; Antonov, V.A.; Radeonychev, Y.V.; Scully, M.O.; Kocharovskaya, O. Transformation of a single-photon field into bunches of pulses. *Phys. Rev. A* **2015**, *92*, 023836. [[CrossRef](#)]
11. Shvyd'ko, Y.V.; Hertrich, T.; Bürck, U.; Gerdau, E.; Leupold, O.; Metge, J.; Rüter, H.D.; Schwendy, S.; Smirnov, G.V.; Potzel, W.; et al. Storage of nuclear excitation energy through magnetic switching. *Phys. Rev. Lett.* **1996**, *77*, 3232. [[CrossRef](#)]
12. Röhlsberger, R.; Schlage, K.; Sahoo, B.; Couet, S.; Rüffer, R. Collective lamb shift in single-photon superradiance. *Science* **2010**, *328*, 1248. [[CrossRef](#)]
13. Röhlsberger, R.; Wille, H.-C.; Schlage, K.; Sahoo, B. Electromagnetically induced transparency with resonant nuclei in a cavity. *Nature* **2012**, *482*, 199. [[CrossRef](#)]
14. Haber, J.; Kong, X.; Strohm, C.; Willing, S.; Gollwitzer, J.; Bocklage, L.; Rüffer, R.; Palfy, A.; Röhlsberger, R. Rabi oscillations of X-ray radiation between two nuclear ensembles. *Nat. Photon.* **2017**, *11*, 720. [[CrossRef](#)]
15. Heeg, K.P.; Kaldun, A.; Strohm, C.; Ott, C.; Subramanian, R.; Lentrodt, D.; Haber, J.; Wille, H.-C.; Goettler, S.; Rüffer, R.; et al. Coherent X-ray–optical control of nuclear excitons. *Nature* **2021**, *590*, 401. [[CrossRef](#)] [[PubMed](#)]
16. Potapkin, V.; Chumakov, A.I.; Smirnov, G.V.; Celso, J.P.; Rüffer, R.; McCammon, C.; Dubrovinsky, L. The ^{57}Fe synchrotron Mössbauer source at the ESRF. *J. Synchrotron Radiat.* **2012**, *19*, 559. [[CrossRef](#)] [[PubMed](#)]
17. Mitsui, T.; Masuda, R.; Seto, M.; Hirao, N. Variable-bandwidth ^{57}Fe synchrotron Mössbauer source. *J. Phys. Soc. Jpn.* **2018**, *87*, 093001. [[CrossRef](#)]
18. Potapkin, V.; McCammon, C.; Dubrovinsky, L.; Glazyrin, K.; Kantor, A.; Kupenko, I.; Prescher, C.; Sinmyo, R.; Smirnov, G.; Popov, S.; et al. No spin transition of ferric iron in the lower mantle. *Nat. Commun.* **2013**, *4*, 1427. [[CrossRef](#)]
19. Kupenko, I.; Dubrovinsky, L.; Dubrovinskaia, N.; McCammon, C.; Glazyrin, K.; Bykova, E.; Boffa Ballaran, T.; Sinmyo, R.; Chumakov, A.I.; Potapkin, V.; et al. Portable Double-Sided Laser-Heating System for Energy-Domain Mössbauer Spectroscopy at Synchrotron and Single Crystal Diffraction Experiments with Diamond Anvil Cells. *Rev. Sci. Instrum.* **2012**, *83*, 124501. [[CrossRef](#)]
20. Prescher, C.; Dubrovinsky, L.; Bykova, E.; Kupenko, I.; Glazyrin, K.; Kantor, A.; McCammon, C.; Mookherjee, M.; Nakajima, Y.; Miyajima, N.; et al. High Poisson's ratio of Earth's inner core explained by carbon alloying. *Nat. Geosci.* **2015**, *8*, 220. [[CrossRef](#)]
21. Potapkin, V.; Chumakov, A.I.; Smirnov, G.V.; Rüffer, R.; McCammon, C.; Dubrovinsky, L. Angular, spectral, and temporal properties of nuclear radiation from a ^{57}Fe synchrotron Mössbauer source. *Phys. Rev. A* **2012**, *86*, 053808. [[CrossRef](#)]
22. Smirnov, G.V.; Bürck, U.; Chumakov, A.I.; Baron, A.Q.R.; Rüffer, R. Synchrotron Mössbauer source. *Phys. Rev. B* **1997**, *55*, 5811. [[CrossRef](#)]
23. Smirnov, G.V. Synchrotron Mössbauer source of ^{57}Fe radiation. *Hyperfine Interact.* **2000**, *125*, 91–112. [[CrossRef](#)]
24. Mitsui, T.; Hirao, N.; Ohishi, Y.; Masuda, R.; Nakamura, Y.; Enoki, H.; Sakaki, K.; Seto, M. Development of an energy-domain ^{57}Fe -Mössbauer spectrometer using synchrotron radiation and its application to ultrahigh-pressure studies with a diamond anvil cell. *J. Synchrotron Radiat.* **2009**, *16*, 723. [[CrossRef](#)] [[PubMed](#)]
25. Zhang, X.; Liao, W.-T.; Kalachev, A.; Shakhmuratov, R.; Scully, M.; Kocharovskaya, O. Nuclear quantum memory and time sequencing of a single γ photon. *Phys. Rev. Lett.* **2019**, *123*, 250504. [[CrossRef](#)] [[PubMed](#)]
26. Radeonychev, Y.V.; Tokman, M.D.; Litvak, A.G.; Kocharovskaya, O. Acoustically induced transparency and generation of multifrequency radiation. *Laser Phys.* **2003**, *13*, 1308.
27. Radeonychev, Y.V.; Tokman, M.D.; Litvak, A.G.; Kocharovskaya, O. Acoustically induced transparency in optically dense resonance medium. *Phys. Rev. Lett.* **2006**, *96*, 093602. [[CrossRef](#)] [[PubMed](#)]
28. Mkrtchyan, A.R.; Arutyunyan, G.A.; Arakelyan, A.R.; Gabrielyan, R.G. Modulation of Mössbauer radiation by coherent ultrasonic excitation in crystals. *Phys. Stat. Sol.* **1979**, *92*, 23. [[CrossRef](#)]
29. Shvyd'ko, Y.V.; Smirnov, G.V. Enhanced yield into the radiative channel in Raman nuclear resonant forward scattering. *J. Phys. Condens. Matter.* **1992**, *4*, 2663. [[CrossRef](#)]
30. Smirnov, G.V.; Bürck, U.; Arthur, J.; Popov, S.L.; Baron, A.Q.R.; Chumakov, A.I.; Ruby, S.L.; Potzel, W.; Brown, G.S. Nuclear Exciton Echo Produced by Ultrasound in forward Scattering of synchrotron radiation. *Phys. Rev. Lett.* **1996**, *77*, 183. [[CrossRef](#)]
31. Smirnov, G.V.; Potzel, W. Perturbation of nuclear excitons by ultrasound. *Hyperfine Interact.* **1999**, *123*, 633–663. [[CrossRef](#)]
32. Schindelmann, P.; van Bürck, U.; Potzel, W.; Smirnov, G.V.; Popov, S.L.; Gerdau, E.; Shvyd'ko, Y.V.; Jäschke, J.; Rüter, H.D.; Chumakov, A.I.; et al. Radiative decoupling and coupling of nuclear oscillators by stepwise doppler-energy shifts. *Phys. Rev. A* **2002**, *65*, 023804. [[CrossRef](#)]
33. Radeonychev, Y.V.; Khairulin, I.R.; Vagizov, F.G.; Scully, M.; Kocharovskaya, O. Observation of acoustically induced transparency for γ -ray photons. *Phys. Rev. Lett.* **2020**, *124*, 163602. [[CrossRef](#)]
34. Khairulin, I.R.; Antonov, V.A.; Radeonychev, Y.V.; Kocharovskaya, O. Ultimate capabilities for compression of the waveform of a recoilless γ -ray photon into a pulse sequence in an optically deep vibrating resonant absorber. *Phys. Rev. A* **2018**, *98*, 043860. [[CrossRef](#)]

35. Antonov, V.A.; Radeonychev, Y.V.; Kocharovskaya, O. γ -ray-pulse formation in a vibrating recoilless resonant absorber. *Phys. Rev. A* **2015**, *92*, 023841. [[CrossRef](#)]
36. Khairulin, I.R.; Radeonychev, Y.V.; Antonov, V.A.; Kocharovskaya, O. Acoustically induced transparency for synchrotron hard X-ray photons. *Sci. Rep.* **2021**, *11*, 7930. [[CrossRef](#)]
37. Radeonychev, Y.V.; Antonov, V.A.; Vagizov, F.G.; Shakhmuratov, R.N.; Kocharovskaya, O. Conversion of recoilless γ radiation into a periodic sequence of short intense pulses in a set of several sequentially placed resonant absorbers. *Phys. Rev. A* **2015**, *92*, 043808. [[CrossRef](#)]
38. Ambrosy, A.; Holdik, K. Piezoelectric PVDF films as ultrasonic transducers. *J. Phys. E Sci. Instrum.* **1984**, *17*, 856. [[CrossRef](#)]
39. Kuznetsova, E.; Kolesov, R.; Kocharovskaya, O. Compression of γ -ray photons into ultrashort pulses. *Phys. Rev. A* **2003**, *68*, 043825. [[CrossRef](#)]